Effect of Coherence on All-Optical Signal Amplification by Supercontinuum Generation

MIKKO NÄRHI[1,*], GÜNTER STEINMEYER[2], AND GOËRY GENTY[1]

[1] Laboratory of Photonics, Tampere University of Technology, Tampere, FI-33720, Finland
[2] Max Born Institute, Humboldt University, Berlin, postcode, Germany
[*] Corresponding author: mikko.narhi@tut.fi

Compiled February 17, 2017

We demonstrate 47 dB all-optical signal amplification of weakly amplitude modulated (-60 dBc) pulse train from a Ti:Sapphire oscillator (FWHM $\approx$ 190 fs) exploiting the sensitivity of supercontinuum generation to input power fluctuations. We also study the effect of supercontinuum coherence to signal reconstruction and map the amplification factors over a wide range of parameters. Soliton-dispersive wave coupling is shown to be a key element in the amplification mechanism.

OCIS codes: *(190.7110) Ultrafast nonlinear optics; (190.4370) Nonlinear optics, fibers; (070.7145) Ultrafast processing.*

http://dx.doi.org/10.1364/ao.XX.XXXXXX

1. INTRODUCTION

Optical signal processing holds great promise to help meet the ever-growing demand on data transfer capacities globally [1]. The main benefit would be achieved in the need for less optical-electrical-optical conversions but the techniques could potentially lead to lower power consumption in some applications [2]. Various functionalities from optical tapped delays/finite impulse response filters [3, 4], optical time division multiplexing [5] and signal regeneration on chip [6, 7] have already been demonstrated among many others. In addition to these, regeneration of amplitude modulated signals all optically could be useful, in addition to optical communications, for research setups such as pump-probe spectroscopy requiring high sensitivities for sensing weak amplitude variations.

Indeed, previous work has also demonstrated amplification of amplitude modulated signals in fibers by 20 times (13 dB) by using the nonlinear effects of self-phase modulation (SPM) and Raman self-frequency shift (RSFS) [8, 9]. In a recent article the combination of these two and other nonlinear effects occurring during supercontinuum generation (SCG) were exploited to reach extremely high amplifications of up to 60 dB for a weakly modulated signal (-70 dBc) [10]. The experiment in ref. [10] utilized few cycle (8 fs) pulses for supercontinuum generation ensuring a high coherence due to a broad bandwidth of the input pulse (or a low soliton number input pulse) [11, 12]. This results in an amplification mechanism that is robust and straightforward to understand due to the deterministic soliton fission causing the supercontinuum generation. A small variation in the input power will cause the solitons to be ejected at different frequencies/velocities which is then transferred in an enhanced manner to the soliton's corresponding dispersive wave. When choosing the observed wavelength properly at the fiber output this can lead to massive signal amplification [10].

In this letter we study more thoroughly the possibility of using the same approach as in [10] with longer duration pulses, when the SCG is not fully deterministic (i.e. coherent) anymore. We explore the coherence dependent effects on this signal regeneration mechanism by controlling the input pulse power and thus varying the degree of coherence for the resulting SC from fully coherent to partially coherent and finally incoherent cases [12, 13]. We also map the amplification factors throughout the whole SC spectrum and verify the physical amplification mechanism based on the soliton-dispersive wave (DW) coupling experimentally.

2. EXPERIMENTAL METHODS

The experimental setup for the signal amplification was similar to that of the one used in [10], only the laser was changed. Simplified illustration of the amplification scheme can be found in figure 1. In these experiments additional measurements by frequency resolved optical gating (FROG) [14] and a delayed Michelson interferometer [12] were used to characterize the input pulse duration and SC coherence respectively.

Soliton fission and modulation instability are the main nonlinear processes affecting SC generation when seeding with few hundred femtosecond pulses in the anomalous dispersion regime [11]. The deterministic soliton fission is competing with the noise influenced modulation instability whose strength grows with increasing seed pulse peak power. This allows for simple tuning of the SC coherence via power adjustment. The peak powers for the coherent, partially coherent and incoherent SC were approximately 240 W, 750 W and 1000 W respectively.

A. Input characterization

The seed for SC generation was Spectra Physics Tsunami Ti:Sapphire laser operating at 798 nm with 80 MHz repetition rate. The pulses were amplitude modulated with a quartz based acousto-optic frequency shifter (custom order from Brimrose) with a square wave signal at 5 MHz. The input pulses injected into the 68.5 cm length PCF (NL-PM-750 by NKT Photonics, with $\gamma_{\mathrm{NL}} = 0.1\ (\mathrm{Wm})^{-1}$ and $\beta_2(\omega_0) = -8.95 \times 10^{-27}\ \mathrm{s}^2/\mathrm{m}$) were characterized with second harmonic generation FROG [14] and the pulse train power modulation was simultaneously recorded from a reflection with a standard silicon photodetector (DET10-A, ThorLabs) and an oscilloscope/RF spectrum analyzer.

The FROG retrieval yielded a 190 fs FWHM chirped pulse with time-bandwidth product of 1.6 after the acousto-optic module. Amplitude modulation of the peak power was ≈ -60 dBc varying within a few dB from measurement to measurement.

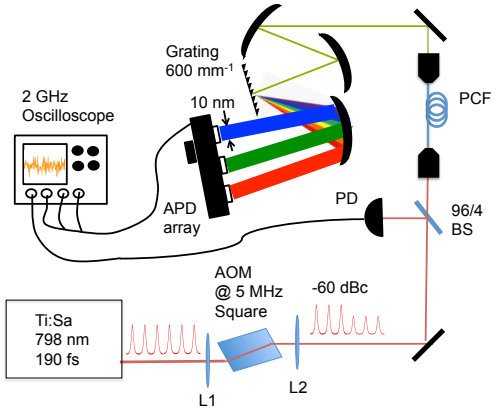

Fig. 1. Experimental setup schematic. AOM = Acousto-optic modulator, PD = Photo detector, BS = Beam splitter, PCF = Photonic Crystal Fiber, APD = Avalanche photodiode, L1 = 75 mm focusing achromatic lens, L2 = 50 mm collimating lens. SHG FROG for pulse characterization and Michelson interferometer for coherence characterization not shown for clarity.

B. Output SC characterization

The fiber output SC was spectrally dispersed in a self-built Czerny-Turner spectrograph ($f = 17.5$ cm) with an avalanche photodiode array (APD, Hamamatsu S8550) in the detector plane. Three channels of the APD array (i.e. three separate SC wavelengths with ≈ 10 nm bandwidth) and the reference signal from the initial modulation were then simultaneously recorded with a 2 GHz real-time oscilloscope (LeCroy WaveRunner 204Xi). The amplification factors for the entire SC spectrum were recorded by tilting the spectrograph grating resulting in new wavelengths at the detector plane and repeating the above measurement. The APD was placed so that the spacing between recorded amplification factors by neighbouring APD pixels was roughly 20 nm to ensure that same spectral regions are not recorded in consecutive measurements. The wavelengths were checked prior to each measurement with the help of a flip mirror and an external spectrometer.

This procedure was repeated for all of the three cases with varying coherence that were achieved by power adjustment of the input pulse. For each wavelength the signal was recorded for about 1 ms and contained roughly 80 000 pulses, ensuring that the statistical properties will be similar for the less coherent SC when varying the angle of the grating.

Cross-correlation FROG [15] was used for the measurement of the partially coherent SC spectrogram to reveal the soliton-DW coupling. The 1mm thick BBO crystal was rapidly dithered (≈ 100 Hz) with a galvanometer scanner to allow for a better phase-matching over the wide SC bandwidth [15, 16]. The gate pulse was a near transform limited output from the Ti:Sapphire with a 66 fs duration (TBP=0.42) characterized with SHG FROG. The sum-frequency generation signal of the gate and SC was integrated over 200 ms (≈ 20 dithering cycles) with a fiber based spectrometer (Avantes 2048L). Only the partially coherent FROG trace was recorded as it showed the highest amplification and clearly identifies the soliton-DW coupling which is blurred due to averaging over the varying single-shot spectra in the incoherent case and not separated enough in the coherent case. The experimental spectrogram is shown in figure 2 highlighting the soliton and dispersive waves.

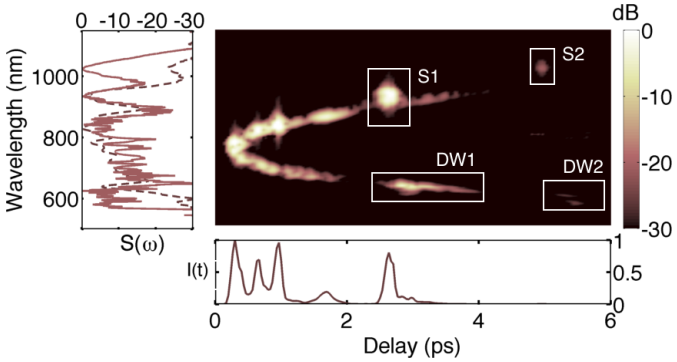

Fig. 2. Experimental XFROG spectrogram and corresponding time and frequency marginals (obtained by integration of the spectrogram) for a partially coherent SC. The dashed line is the frequency marginal and solid line presents the spectrum measured by OSA in the left inset. S1 and S2 are ejected fundamental solitons, DW1 and DW2 their corresponding dispersive waves. S2 and DW2 appear fainter than they should because of weak phase-matching even with angle dithering.

Coherence properties were characterized by a free-space delayed Michelson interferometer where the delay difference between the two arms was equal to the repetition rate of the laser (≈ 3.75m). The interferometer output was then recorded with an optical spectrum analyzer (ANDO AQ6315B) yielding a spectral interferogram from which the first order coherence properties can be infered from visibility calculations [17].

3. RESULTS AND DISCUSSION

A. Coherent supercontinuum

We start with the coherent case with pulse peak power of approximately 240 W with a soliton order of $N = T_0\sqrt{\gamma P_p/|\beta_2|} = 10$. This results in an SC spectrum extending from roughly 625 nm to 950 nm (-30 dB bandwidth). The spectrum is shown in the lower left corner of figure 3 below. The measured first-order spectral coherence function is plotted in red in the upper left figure showing a uniform visibility in the measured interference fringes indicating a high coherence (average degree of coherence $\bar{g}_{12} \approx 0.86$). Unity value is not obtained due to technical noise of the interferometer.

In the same plot with the coherence function are the recorded discrete amplification factors (blue triangles) at 10 nm spectral

window bins.

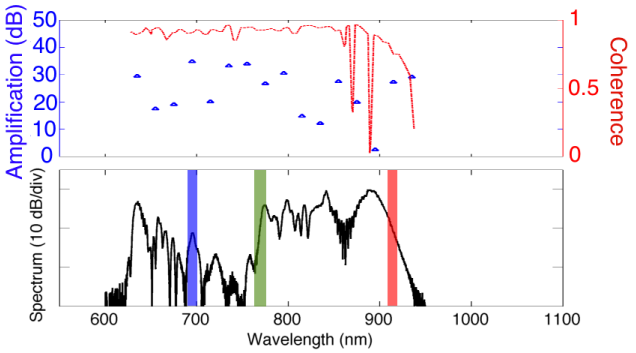

Fig. 3. Coherent SC. **Up:** Coherence function (red) and amplification factors (blue), **Down:** Recorded SC spectrum with three spectral bins highlighted that are plotted in figure 4.

We have also chosen three examples out of the recorded amplification factors to illustrate how the signal reconstruction works. The measured oscilloscope traces were processed with the help of a modified Takeda algorithm [18]. The uppermost (yellow) insets show the recorded RF spectrum of the input pulse and attempted time domain signal modulation retrieval. The modulation peak at 5 MHz is barely visible above the detector noise floor of -67 dB and the time domain signal reconstruction shows only noisy fluctuations.

Out of the three examples chosen, the blue curve at 695 nm DW peak shows the most prominent modulation pattern after reconstruction with a 0.2 μs period corresponding to the 5 MHz modulation. This is easily understood by considering the fact that whenever the pulse peak power is lower than the nominal value, the soliton fission process is altered leading to the first ejected soliton experiencing a different Raman shift and thus a different wavelength. Therefore the corresponding DW coupled to the soliton will be shifted outside of our APD spectral window resulting in a near "on-off" modulation at the output.

B. Partially coherent supercontinuum

Increasing the peak power to 750 W ($N = 17$) we see an increase in spectral bandwidth extending from 550 nm 1100 nm at the cost of a decrease in the coherence of the SC, which can be seen in the varying first order coherence function values ($\bar{g}_{12} \approx 0.58$) plotted in figure 5. Similarly to the coherent case also the RF spectra and examples of signal reconstruction at chosen wavelengths are shown in figure 6.

The pulse to pulse fluctuations of the SC are not still not significant and the timing jitter of the solitons is of the order of their duration. This is why the XFROG trace in figure 2 still yields a good picture of the SC temporal evolution. The loss of coherence starts to show in the spectrum at the first and second ejected solitons at 1030 nm and 930 nm for which the MI is starting to perturb the ejection process from shot-to-shot. These random fluctuations in the soliton wavelength and intensity caused by MI manifest themselves as increased noise levels in the measurement.

The highest amplification factor of 47 dB recorded in our experiments was in the partially coherent case at 640 nm in the DW spectral edge highlighted in blue. This is again in agreement with the picture of soliton-DW coupling being sensitive to input power fluctuations and yielding the highest amplifications. The

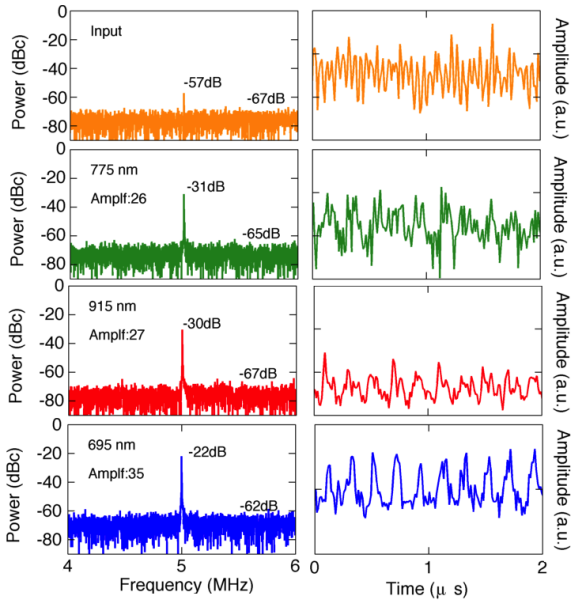

Fig. 4. RF spectra of coherent SC. Yellow is the input pulse train and other colors correspond to the highlighted spectral bins in the spectrum. Right column shows the reconstructed time domain signals.

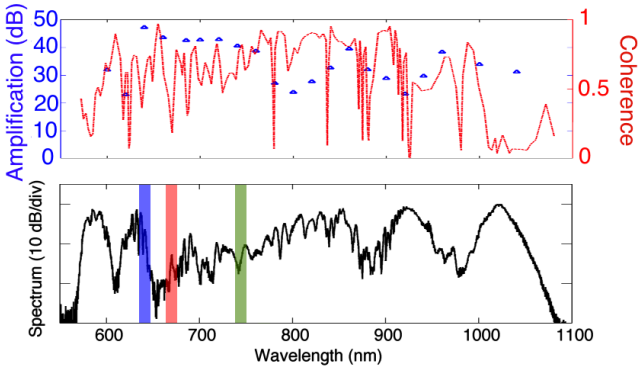

Fig. 5. Partially coherent SC. **Up:** Coherence function (red) and amplification factors (blue), **Down:** Recorded SC spectrum with three spectral bins highlighted that are plotted in figure 6.

modulated signal is clearly visible in the time domain picture of figure 6 with the increased noise degrading the signal shape slightly.

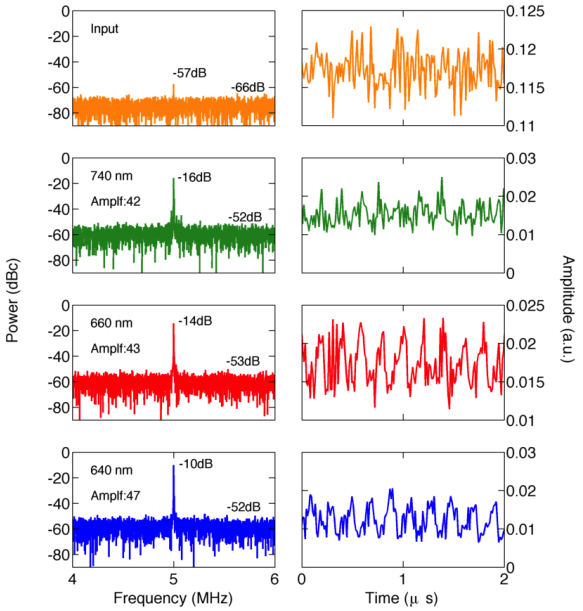

Fig. 6. RF spectra of partially coherent SC. Yellow is the input pulse train and other colors correspond to the highlighted spectral bins in the spectrum. Right column shows the reconstructed time domain signals.

C. Incoherent supercontinuum

As a final example the peak power was set to 1000 W ($N = 20$) resulting in strongly degraded coherence ($\bar{g}_{12} \approx 0.11$) and effectively increasing the soliton timing jitter over a much greater time span than the soliton duration. Correlations between the generated SC spectra are only seen seeded by the pump remains at 800 nm and at the DW edge that has been perturbed the least corresponding to the first ejected soliton. The spectrum extends to over 1100 nm, which is beyond the sensitivity of our APD array and thus it was not plotted in the spectrum above.

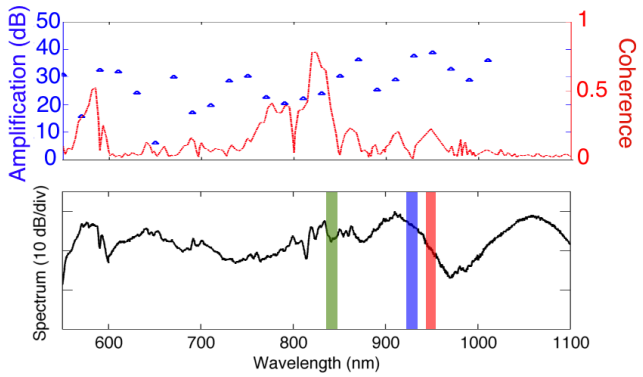

Fig. 7. Incoherent SC. **Up:** Coherence function (red) and amplification factors (blue), **Down:** Recorded SC spectrum with three spectral bins highlighted that are plotted in figure 8.

Even though amplification is still observed, the signal reconstruction does not work for any of the cases because of the increased noise due to loss of coherence.

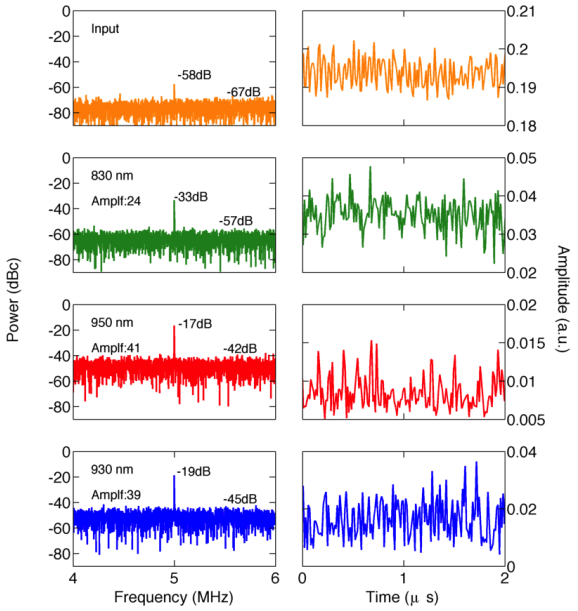

Fig. 8. RF spectra of incoherent SC. Yellow is the input pulse train and other colors correspond to the highlighted spectral bins in the spectrum. Left insets show the reconstructed time domain signals. One can observe the noise floor getting higher in the RF spectra compared to previous cases.

D. Discussion

Even though relatively high amplifications are seen throughout the spectra for all three cases with different coherence properties, increased noise caused degrades the possibility for reliable signal reconstruction. This can be easily observed by comparing the second (green) line of plots in figure 8 and the fourth (blue) line in fig. 6. The first case shows 42 dB amplification whereas the corresponding number is only 35 dB in the latter case. However in the latter case one can easily see the modulation in the temporal signal, whereas it's completetely blurred out by noise in the first case.

The noise level is not only affected by the supercontinuum coherence, but also by the intensity of light and the quantum efficiency of the detector at a given wavelength. The effect of SC coherence on the noise levels can be observed from comparing the average noise noise floor values for all of the wavelengths for varying SC coherences. For the coherent, partially coherent and incoherent cases the mean noise floors over the whole spectra were -71 dBc, -65 dBc and -57 dBc respectively. One can observe a clear increase in the mean noise floor for less coherent SC generation caused by MI induced shot-to-shot fluctuations.

Finally we would like to note, that occasionally when performing the experiments and working with a coherent SC at the first soliton peak around 900 nm wavelength range we observed negative amplifications of few dB. This effect was also observed in the numerical simulations of [10] around the first soliton wavelength and the DW edge of the spectrum. This could correspond to a macroscopical version of amplitude squeezing observed in quantum optics and could prove to be useful in applications where measured amplitude fluctuations would require to be reduced all optically. The details of this mechanism are however beyond the scope of this article.

4. CONCLUSIONS

We have shown that supercontinuum generation process can be used as a signal amplifier without the need of single-cycle pulses and with decreased SC coherence. Varying amplification values within the spectrum can be understood with the help of the overall spectral shape and the associated SCG dynamics.

The success of reconstruction of the amplified signal requires a balance of multiple factors. Firstly the corresponding SC wavelength needs to have enough spectral power and to be coherent enough to keep the general noise floor down. Secondly the wavelength needs to be chosen so that weak modulation of the input pulse can result in a strong enough jitter in the resulting spectrum. This is usually occuring at steep spectral features corresponding to the solitons and their dispersive waves for which the Raman shifts are more prominent.

The reduced requirements on the SCG pump source for signal amplification open up new venues for applications of the system in e.g. pump-probe systems requiring high sensitivity. Furthermore, advances in SCG on chips with low powers could be used to decrease the peak powers required for applying the technique.

FUNDING INFORMATION

Funding. MN acknowledges the support from Kaute foundation.

ACKNOWLEDGMENTS

Acknowledgment. The authors thank L. Orsila and J. Sand for technical support.

REFERENCES

Note that *Optics Letters* does not include journal article titles or full page ranges in the published article. Only the first page is required. However, a fifth informational-only page containing the full references should be included. The informational page does not count toward the length restriction.

REFERENCES

1. A. E. Willner, S. Khaleghi, M. R. Chitgarha, and O. F. Yilmaz, "All-optical signal processing," J. Lightwave Technol. **32**, 660–680 (2014).
2. M. Taubenblatt, "Optical interconnects for high-performance computing," Lightwave Technology, Journal of **30**, 448–457 (2012).
3. S. Khaleghi, M. R. Chitgarha, O. F. Yilmaz, M. Tur, M. W. Haney, C. Langrock, M. M. Fejer, and A. E. Willner, "Experimental performance of a fully tunable complex-coefficient optical fir filter using wavelength conversion and chromatic dispersion," Opt. Lett. **37**, 3420–3422 (2012).
4. J. Sharping, Y. Okawachi, J. van Howe, C. Xu, Y. Wang, A. Willner, and A. Gaeta, "All-optical, wavelength and bandwidth preserving, pulse delay based on parametric wavelength conversion and dispersion," Opt. Express **13**, 7872–7877 (2005).
5. B. J. Eggleton, B. Luther-Davies, and K. Richardson, "Chalcogenide photonics," Nat Photon **5**, 141–148 (2011).
6. O. Boyraz and B. Jalali, "Demonstration of 11db fiber-to-fiber gain in a silicon raman amplifier," IEICE Electronics Express **1**, 429–434 (2004).
7. M. A. Foster, A. C. Turner, J. E. Sharping, B. S. Schmidt, M. Lipson, and A. L. Gaeta, "Broad-band optical parametric gain on a silicon photonic chip," Nature **441**, 960–963 (2006).
8. C. Finot and J. Fatome, "All-optical fiber-based ultrafast amplitude jitter magnifier," Opt. Express **18**, 18697–18702 (2010).
9. C. H. Hage, B. Kibler, and C. Finot, "Fiber-based device for the detection of low-intensity fluctuations of ultrashort pulses," Appl. Opt. **51**, 949–953 (2012).
10. L. Orsila, J. Sand, M. Närhi, G. Genty, and G. Steinmeyer, "Supercontinuum generation as a signal amplifier," Optica **2**, 757–764 (2015).
11. J. M. Dudley, G. Genty, and S. Coen, "Supercontinuum generation in photonic crystal fiber," Rev. Mod. Phys. **78**, 1135–1184 (2006).
12. M. Närhi, J. Turunen, A. T. Friberg, and G. Genty, "Experimental measurement of the second-order coherence of supercontinuum," Phys. Rev. Lett. **116**, 243901 (2016).
13. G. Genty, M. Surakka, J. Turunen, and A. T. Friberg, "Second-order coherence of supercontinuum light," Opt. Lett. **35**, 3057–3059 (2010).
14. R. Trebino, K. W. DeLong, D. N. Fittinghoff, J. N. Sweetser, M. A. Krumbügel, B. A. Richman, and D. J. Kane, "Measuring ultrashort laser pulses in the time-frequency domain using frequency-resolved optical gating," Review of Scientific Instruments **68**, 3277–3295 (1997).
15. X. Gu, L. Xu, M. Kimmel, E. Zeek, P. O'Shea, A. P. Shreenath, R. Trebino, and R. S. Windeler, "Frequency-resolved optical gating and single-shot spectral measurements reveal fine structure in microstructure-fiber continuum," Opt. Lett. **27**, 1174–1176 (2002).
16. P. O'Shea, M. Kimmel, X. Gu, and R. Trebino, "Increased-bandwidth in ultrashort-pulse measurement using an angle-dithered nonlinear-optical crystal," Opt. Express **7**, 342–349 (2000).
17. J. M. Dudley and S. Coen, "Coherence properties of supercontinuum spectra generated in photonic crystal and tapered optical fibers," Opt. Lett. **27**, 1180–1182 (2002).
18. M. Takeda, H. Ina, and S. Kobayashi, "Fourier-transform method of fringe-pattern analysis for computer-based topography and interferometry," J. Opt. Soc. Am. **72**, 156–160 (1982).